CrossMark

Study of advancement to higher temperature membrane distillation

Aoyi Luo*, Noam Lior

Department of Mechanical Engineering and Applied Mechanics, University of Pennsylvania, Philadelphia, PA 19104-6315, USA

ARTICLE INFO

ABSTRACT

It is well known that the mass flux (J) and the membrane thermal efficiency (η) of membrane distillation increase with the feed flow temperature. A comprehensive laminar and turbulent flow model for simulating and evaluating the performance of direct contact membrane distillation (DCMD) when operated at inlet feed temperature ($T_{f,i}$) from 80 °C to 180 °C, higher than the customary maximum of ~80 °C, was developed and used to explain and assess the performance of such high temperature DCMD, as well as the potential associated problems of the needed higher operating pressure, and provide knowledge useful for their future design and optimization. Some of the key results are that raising $T_{f,i}$ from 80 °C to 180 °C, increases J 9.4-fold, and η 2.1-fold, and decreases the specific energy consumption (SEC) 2.9-fold. Raising the flow Reynolds number from 1200 to 7000 increases J 2.6-fold and η by 15%, but SEC increases 2.3-fold. The needed system pressurization does not affect the process performance significantly. The higher operating temperatures also provide more practical opportunities for heat recovery, which could significantly further raise overall system efficiency.

1. Introduction and objectives

Membrane distillation (MD) is recognized as a thermally driven membrane separation process with many advantages [1–7], including the high purity of its product [2,6], as well as lower sensitivity to concentration polarization and fouling when compared to pressure driven membrane separation processes [1], its compact volume [3], and its capability to use low-temperature waste heat and/or renewable energy sources such as solar and geothermal energy. Typical feed solution temperatures for MD are below about 80 °C, which was mostly dictated by the tolerance of the separation membrane polymers. Notwithstanding the above mentioned advantages of using low temperature heat sources, it is widely published and known that the mass flux and the thermal efficiency of MD increase with the feed solution temperature [3,4]. Higher operating temperatures also provide more practical opportunities for heat recovery, which could significantly further raise overall system efficiency. The main objective and novel contribution of this study is therefore to explore the conditions, potential and consequences of raising the temperature above 80 °C for what is (arguably) the most used MD configuration called 'direct contact membrane distillation' (DCMD) in desalination MD, where, as shown in Fig. 1, the warm saline feedwater flows along one side of the separation membrane, while the colder fresh water product flows along its other (permeate) side.

It is noteworthy that while conventional MD, including DCMD, operates below the boiling temperature of the feedwater solution, which for saline water is associated with saturation pressures somewhat higher than atmospheric, increasing with salinity. Since boiling with the associated generation and motion of bubbles will disrupt the MD process (with yet-unknown consequences), operation at temperatures above the boiling temperature are conducted by raising the operating pressure to values above those of saturation corresponding the desired operating temperature. This study therefore also includes examination of pressure effects on the membrane transport.

There is much evidence, from both numerical simulations and experiments, of the above-mention flux and efficiency improvement trend with increasing of the feedwater temperature within the currently used low temperature range. For example, numerical analysis of DCMD has shown that increasing the feed temperature from 40 °C to 80 °C increases the permeate mass flux 4.6-fold and the below-defined membrane thermal efficiency (η) by 16% (from 77.1% to 89.5%) [4].

Furthermore, several experimental studies have been made of the mass flux of MD up to 128 °C at pressures up to 3 atm (~300 kPa), and thus verified the basic feasibility of successful operation at temperatures above the conventional 80 °C and well above atmospheric pressure. Reference [8] is a study of DCMD of a 1% NaCl solution using flat polytetrafluoroethylene (PTFE) membranes, and measured that raising the feed temperature from 80 °C to 95 °C elevated the vapor mass flux 4.6-fold, and that raising it from 110 °C to 128 °C elevated the vapor mass flux 1.9-fold. In [9] they used PTFE hollow-fiber DCMD and measured that raising the feed temperature

---

Nomenclature

A	membrane area [m^2]
B	geometric factor [dimensionless]
C	membrane permeability [kg/(m^2·s·Pa)]
C_v	specific heat capacity at constant volume [J/(K·kg)]
C_p	specific heat capacity at constant pressure [J/(K·kg)]
d_p	membrane pore size [μm]
D	diffusion coefficient [m^2/s]
DCMD	direct contact membrane distillation
Eu	Euler number [dimensionless]
$\dot{E}_{des}$	exergy destruction rate [W]
$\dot{E}_{flow}$	rate of the overall flow exergy transfer [W]
$\dot{E}_{heat}$	thermal energy input rate needed to heat the fluid [W]
$\dot{E}_{input}$	exergy input rate [W]
$\dot{E}_{input}$	energy input rate [W]
$\dot{E}_{output}$	exergy output rate [W]
h_{ch}	channel height [m]
h_f	convective heat transfer coefficient of the feed stream [W/(m^2·K)]
h_m	conduction heat transfer coefficient of the membrane [W/(m^2·K)]
$h_{p.}$	convective heat transfer coefficient of the permeate stream [W/(m^2·K)]
H_m	total heat transfer coefficient of the membrane [W/(m^2·K)].
J	mass flux [kg/(m^2·s)]
k	thermal conductivity [W/(m·K)]
k_g	thermal conductivity of the gas present in the pores [W/(m·K)]
k_{me}	effective membrane thermal conductivity [W/(m^2·K)]
k_s	membrane material thermal conductivity [W/(m^2·K)]
LEP	liquid entry pressure [Pa]
l_{ch}	module length [m]
M	molecular weight of vapor [kg/mol]
MD	membrane distillation
$\dot{m}_d$	mass flow rate of the distillate [kg/s]
P	total pressure [Pa]
PP	polypropylene
Pr	Prandtl number [dimensionless]
PTFE	polytetrafluoroethylene
PVDF	polyvinylidene fluoride
$p_{f,m}$	vapor pressure at the membrane feed-side surface [Pa]
$p_{p.,m}$	vapor pressure at the membrane permeate-side surface [Pa]
p_{air}	average partial pressure of the non-condensable gas in the membrane [Pa]
$p_{v,w}$	vapor pressure of pure water [Pa]
$p_{v,sw}$	vapor pressure of sea water [Pa]
p_{sat}	saturation pressure at the feed inlet [Pa]
$q_c^{''}$	heat flux across the membrane by conduction [W/m^2].
$q_v^{''}$	heat flux across the membrane by evaporation [W/m^2].
$q_{mem}^{''}$	heat flux across the membrane [W/m^2].
$q_t^{''}$	total heat flux across the membrane [W/m^2].
r	average pore radius [m]
R	ideal gas constant [J/(mol·K)]
Re	Reynolds number [dimensionless]
S	salinity [g/kg]
SEC	specific energy consumption [J/kg]
Sc	Schmidt number [dimensionless]
SXC	specific exergy consumption [J/kg]
T	temperature [K]
T_g	glass transition temperature [K]
u	velocity [m/s]
$\dot{V}$	volumetric flow rate [m^3/s].
w	mass fraction [%]
$\dot{W}_{pump}$	pump work needed to pressurized the fluid [W].

Greek

γ_L	liquid surface tension [N/m]
δ	membrane thickness [m]
ΔH_{fg}	specific enthalpy of vaporization [J/kg]
ΔJ	difference between J corresponds to the highest $T_{f,i}$ and J corresponds to the lowest $T_{f,i}$ [kg/(m^2·s)]
ΔP_{inter}	pressure difference at liquid/gas interface [Pa].
$\Delta T_{f,i}$	difference between the highest $T_{f,i}$ and the lowest $T_{f,i}$ [K]
ε	membrane porosity [dimensionless]
θ	membrane/liquid contact angle [° or rad]
η	membrane thermal efficiency [dimensionless]
μ	viscosity [Pa·s]
ρ	density of the fluid [kg/m^3]
ψ	exergy efficiency [dimensionless]
γ	pump efficiency [dimensionless]
χ	membrane tortuosity [dimensionless]
Ω	relative heat transfer resistance [dimensionless]

Subscript

f,i	feed inlet
f,m	feed/membrane interface
i	inlet
mem	membrane
p,i	permeate inlet
p,m	permeate/membrane interface
pro	product
0	dead state

Superscript

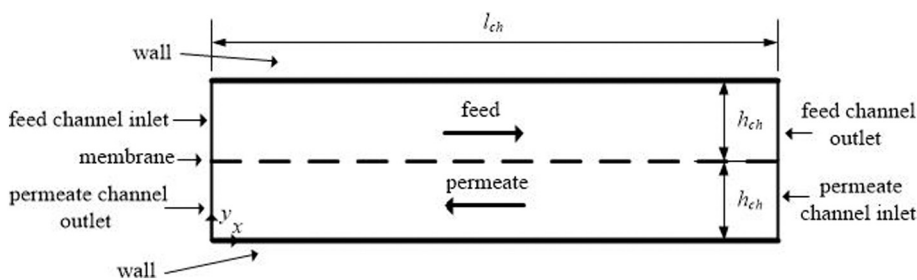|	
*	dimensionless value

Fig. 1. Schematic of the studied DCMD module.

Table 1
Prior studies of the mass flux and its increase as a function of the feed temperature.

Reference	$T_{f,i}$, °C	$T_{p,i}$, °C	J, kg/(m²·h)	$\Delta J/\Delta T_{f,i}$ kg/(m²·h·°C)	Feed aqueous solution
Alklaibi & Lior [4]	40 → 80	20	6.3 → 28.9	0.57	2.5% NaCl
Singh & Sirkar [8]	80 → 95	25	14.5 → 66	3.4	1% NaCl
Singh & Sirkar [8]	110 → 128	25	105 → 195	5	1% NaCl
Singh & Sirkar [9]	85 → 95	29	6.8 → 15	0.82	1% NaCl
Singh & Sirkar [9]	108 → 118	29	68 → 115	4.7	1% NaCl

from 85 °C to 95 °C elevated the vapor mass flux 2.2-fold, and that raising it from 108 °C to 118 °C elevated the vapor mass flux 1.7-fold. The experimental results and average mass flux increase per °C of temperature raise of the feed of these studies are summarized in Table 1 where ΔJ is the difference between the J corresponding to the highest $T_{f,i}$ and J corresponding to the lowest $T_{f,i}$, and $\Delta T_{f,i}$ is difference between the highest $T_{f,i}$ and the lowest $T_{f,i}$. It can be seen that high temperature MD over 100 °C results in higher mass flux increase per unit feed temperature increase than at lower feed temperatures.

Membranes for the customary low-temperature MD are made of polymers that may be practically inapplicable at higher temperatures, which is the main reason that typical MD processes were conducted at temperatures below about 90 °C. A way to raise the operating temperature is by using different membrane materials, such as higher temperature polymers, ceramics and composites. Many studies have investigated utilizing ceramic membrane for MD but only below 100 °C [10–17]. Furthermore, membrane fabrication technology is continuously improving, and membranes can now be fabricated with increasingly extraordinary mechanical properties and contact angles [18,19]. High temperature MD thus also serves as an incentive for developing correspondingly improved membranes.

As one of the anonymous Reviewers remarked, use of saline water temperatures above 100 °C may create an opportunity to use water vapor transport membranes, but this was not studied in this paper. For example, GORE-TEX® membranes were indeed experimentally used for MD but eventually found much more lucrative markets in the garment industry.

It is noteworthy that raising the temperature of all thermal water desalination processes, including MD, makes them increasingly vulnerable to precipitation of salts such as calcium carbonate, magnesium hydroxide, and calcium phosphate, if they are present in the feed water, especially when the temperature reaches the solution saturation conditions. The solubility of calcium carbonate, magnesium hydroxide, and calcium phosphate decreases with temperature [20]. This precipitation may cause excessive fouling of the membranes. High temperature DCMD can be used, however, if the feed water does not originally contain such species, or by pretreating the feed water (such as by coagulation, precipitation, nano-filtration, thermal water softening, use of antiscalants and pH control [20–22]) if it does.

In this study, a flat sheet DCMD module using a PTFE membrane with saline water feed inlet temperature from 80 °C to 180 °C was investigated by fundamental numerical simulation. A comprehensive and validated simulation model for these higher-than-customary temperatures was developed as described in Section 2 below and was used to explain and assess the performance of such high temperature DCMD, as well as some of the potential associated problems. It also provides useful knowledge for future design and optimization of high temperature DCMD. The quantitative results for MD at these higher temperatures are, to the best of our knowledge, the first in the literature.

2. Model development

2.1. The computational domain

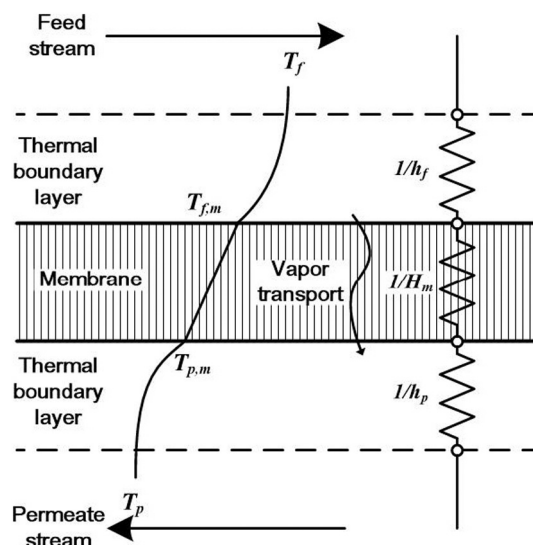Fig. 1 shows the schematic of the analyzed DCMD module. The feed

Fig. 2. Qualitative depiction of the temperature profile, vapor mass transport, and heat transfer resistance analog in DCMD.

stream and permeate stream are in counterflow. The porous hydrophobic membrane between the feed and permeate streams allows only the generated vapor to pass through it. The module interface with its surroundings is assumed to be adiabatic, thus the bottom and top walls in Fig. 1 are adiabatic.

To evaluate the performance of this DCMD module (the performance criteria, including the mass flux membrane thermal efficiency, total heat flux, relative heat transfer resistance, exergy efficiency, specific exergy consumption, specific energy consumption, described in Section 7), it is needed to calculate the temperature, flow, pressure, and concentration fields in the DCMD module, for which we developed the below-described comprehensive model that includes the transport in the membrane and the participating fluids.

2.2. The transport in the analyzed DCMD process

The temperature profile, vapor mass transport, and heat transfer resistance analog in DCMD are qualitatively described in Fig. 2, and the model for analyzing the transport in the DCMD module is described below.

As shown in Fig. 2, the thermal driving force for the evaporative separation process is the temperature difference between the warm feedwater solution and the colder permeate stream, $(T_f - T_p)$. Heat is transferred from and through the warm feedwater at temperature T_f to the upper surface of the membrane, where evaporation starts, and heat is transferred through the membrane and then through and to the permeate stream, which is kept at the colder temperature T_p by supply of fresh water coolant, and in which condensation of the transported vapor takes place. The explanation of the shown serial heat transfer resistances follows.

The heat first is transferred across the feed stream boundary layer is expressed as:

$$q_f^{'} = h_f(T_f - T_{f,m}),\qquad(1)$$

where all the variables used in the equations of this paper are defined in the Nomenclature at its end.

Next, the heat is transferred across the membrane in two parallel paths, one is heat conduction through the membrane structural material and the gas contained in the membrane pores, and the other is the latent heat of evaporation of the vapor mass flux, expressed by Eq. (2). It is noteworthy that the heat transferred by the first, conductive, path has negligible contribution to the vapor mass flux and is thus considered to be an energy loss. The total heat transfer rate across the membrane thus is

$$q_{mem}^{''} = q_c^{''} + q_v^{''} = J\Delta H_{fg} + h_m(T_{f,m} - T_{p,m}) = H_m(T_{f,m} - T_{p,m}), \quad (2)$$

and the total heat transfer coefficient across the membrane (H_m) is thus defined as:

$$H_m = \frac{q_{mem}^{''}}{T_{f,m} - T_{p,m}} = \frac{J\Delta H_{fg} + h_m(T_{f,m} - T_{p,m})}{T_{f,m} - T_{p,m}} \quad (3)$$

where h_m is calculated by:

$$h_m = \frac{k_{me}}{\delta} = \frac{\varepsilon k_g + (1-\varepsilon)k_s}{\delta} \quad (4)$$

Heat is then transferred across the permeate stream boundary layer:

$$q_p^{''} = h_p(T_{p,m} - T_p) \quad (5)$$

At steady state, and ignoring heat losses from the membrane or module periphery, the total cross-membrane heat flux is:

$$q_t^{''} = q_f^{''} = q_{mem}^{''} = q_p^{''} \quad (6)$$

Combining Eqs. (1) to (6), the total heat flux is:

$$q_t^{''} = \frac{T_f - T_p}{\frac{1}{h_f} + \frac{1}{H_m} + \frac{1}{h_p}} \quad (7)$$

The mass flux (J) of the distillate across the membrane is expressed by:

$$J = C(p_{f,m} - p_{p,m}) \quad (8)$$

Using a correlation from Ref. [23], the temperature and concentration dependent saturated vapor pressure is calculated by:

$$\ln(p_{v,w}) = a_1/T + a_2 + a_3 T + a_4 T^2 + a_5 T^3 + a_6 \ln(T) \quad (9)$$

$$\frac{p_{v,w}}{p_{v,sw}} = 1 + 0.57357\left(\frac{S}{1000 - S}\right) \quad (10)$$

This correlation valid for $273.15 \leq T \leq 473.15\,K$ and $0 \leq w \leq 0.24$.

The vapor mass flux through the membrane is evaluated by using the dusty gas model (DGM) for its permeability [2], which becomes simplified to Knudsen-molecular diffusion because both sides of the membrane are kept at approximately the same total pressure. The flux is therefore expressed as [2]:

$$J = \left\{\left[\frac{2}{3}\frac{r\varepsilon}{\chi\delta}\left(,\frac{8M}{\pi RT_{mem}}\right)^{\frac{1}{2}}\right]^{-1} + \left(\frac{\varepsilon}{\chi\delta}\frac{DM}{RT_{mem}}\frac{P_{mem}}{p_{air}}\right)^{-1}\right\}^{-1}(p_{f,m} - p_{p,m}), \quad (11)$$

noting that the driving force for the vapor flux is the vapor pressure difference ($p_{f,m} - p_{p,m}$) rather than the total pressure, and vapor pressure is a function of water temperature and concentration. As the feed temperature is increase, the vapor pressure increases exponentially.

3. The governing transport equations in the fluids

This section describes the governing transport equations that are solved to find the needed temperature, flow, pressure and concentration fields in the DCMD module. The variables are made dimensionless as follows:

$$x^* = \frac{x}{h_{ch}},\ y^* = \frac{y}{h_{ch}},\ u^* = \frac{u}{u_{f,i}},\ v^* = \frac{v}{u_{f,i}},\ p^* = \frac{p}{p_{sat}},$$
$$T^* = \frac{T - T_{p,i}}{T_{f,i} - T_{p,i}},\ w^* = \frac{w}{w_i},\ \mu^* = \frac{\mu}{\mu_{f,i}},\ k^* = \frac{k}{k_{f,i}},\ D^* = \frac{D}{D_{f,i}} \quad (12)$$

The DCMD module is analyzed in this study for both laminar and turbulent stream flows, the latter to explore the potential of turbulence for improving the heat and mass transport in the liquid streams. For the laminar flow, the continuity, momentum, energy and species equations

in dimensionless form are:

$$\frac{\partial u^*}{\partial x^*} + \frac{\partial v^*}{\partial y^*} = 0 \quad (13)$$

$$u^*\frac{\partial u^*}{\partial x^*} + v^*\frac{\partial u^*}{\partial y^*} = -Eu\frac{\partial p^*}{\partial x^*} + \frac{1}{2\,Re}\left[\frac{\partial}{\partial x^*}\left(\mu^*\frac{\partial u^*}{\partial x^*}\right) + \frac{\partial}{\partial y^*}\left(\mu^*\frac{\partial u^*}{\partial y^*}\right)\right] \quad (14)$$

$$u^*\frac{\partial v^*}{\partial x^*} + v^*\frac{\partial v^*}{\partial y^*} = -Eu\frac{\partial p^*}{\partial y^*} + \frac{1}{2\,Re}\left[\frac{\partial}{\partial x^*}\left(\mu^*\frac{\partial v^*}{\partial x^*}\right) + \frac{\partial}{\partial y^*}\left(\mu^*\frac{\partial v^*}{\partial y^*}\right)\right] \quad (15)$$

$$u^*\frac{\partial T^*}{\partial x^*} + v^*\frac{\partial T^*}{\partial y^*} = \frac{1}{2RePr}\left[\frac{\partial}{\partial x^*}\left(k^*\frac{\partial T^*}{\partial x^*}\right) + \frac{\partial}{\partial y^*}\left(k^*\frac{\partial T^*}{\partial y^*}\right)\right] \quad (16)$$

$$u^*\frac{\partial w^*}{\partial x^*} + v^*\frac{\partial w^*}{\partial y^*} = \frac{1}{2\,Re\,Sc}\left[\frac{\partial}{\partial x^*}\left(D^*\frac{\partial w^*}{\partial x^*}\right) + \frac{\partial}{\partial y^*}\left(D^*\frac{\partial w^*}{\partial y^*}\right)\right] \quad (17)$$

where Re, Eu, Pr, Sc are the Reynolds, Euler, Prandtl and Schmidt numbers, respectively, at the feed side:

$$Re = \frac{\rho u_{f,i} 2h_{ch}}{\mu_{f,i}} \quad (18)$$

$$Eu = \frac{P}{\rho u_{f,i}^2} \quad (19)$$

$$Pr = \frac{\mu_{f,i} C_p}{k_{f,i}} \quad (20)$$

$$Sc = \frac{\mu_{f,i}}{\rho D_{f,i}} \quad (21)$$

For the turbulent flow, a realizable $k - \varepsilon$ model is used since it is a widely used turbulence model to predict the transport of turbulent flow, with the governing equations from Ref. [24].

The correlations for the saline water properties (density, thermal conductivity, and viscosity) are from [23] which are valid for the range $273.15K \leq T \leq 453.15K$ and $0 \leq w \leq 0.16$.

4. The boundary conditions

The feed channel inlet ($x^* = 0, 1 \leq y^* \leq 2$)

$$u^*(0, y^*) = 1 \quad (22)$$

$$v^*(0, y^*) = 0 \quad (23)$$

$$T^*(0, y^*) = 1 \quad (24)$$

$$w^*(0, y^*) = 1 \quad (25)$$

The permeate channel inlet ($x^* = \frac{l_{ch}}{h_{ch}}, 0 \leq y^* \leq 1$)

$$u^*\left(\frac{l_{ch}}{h_{ch}}, y^*\right) = -1 \quad (26)$$

$$v^*\left(\frac{l_{ch}}{h_{ch}}, y^*\right) = 0 \quad (27)$$

$$T^*\left(\frac{l_{ch}}{h_{ch}}, y^*\right) = 0 \quad (28)$$

$$w^*\left(\frac{l_{ch}}{h_{ch}}, y^*\right) = 0 \quad (29)$$

The feed channel outlet ($x^* = \frac{l_{ch}}{h_{ch}}, 1 \leq y^* \leq 2$)

$$p^*\left(\frac{l_{ch}}{h_{ch}}, y^*\right) = 2 \quad (30)$$

The permeate channel outlet ($x^* = 0, 0 \leq y^* \leq 1$)

$$p^*(0, y^*) = 2 \tag{31}$$

The membrane interface of the feed channel ($0 \leq x^* \leq \frac{l_{ch}}{h_{ch}}$, $y^* = 1^+$)

$$u^*(x^*, 1^+) = 0 \tag{32}$$

$$v^*(x^*, 1^+) = 0 \tag{33}$$

$$- k^* \frac{\partial T^*}{\partial y^*}(x^*, 1^+) = \frac{h_{ch}(q_v^{''} + q_c^{''})}{k_i(T_{f,i} - T_{p,i})} \tag{34}$$

$$- D^* \frac{\partial (1 - w^*)}{\partial y^*}(x^*, 1^+) = \frac{J h_{ch}}{D_i} \tag{35}$$

In the fluid simulation, the geometric configuration of the membrane and the transport within it are not included in the fluid computational domain, and are instead calculated by Eqs. (2) to (4) and Eqs. (8) to (11), so the membrane serves as boundary conditions for the feed and permeate streams in the computational domain.

At $y^* = 1$ in the fluid computational domain, two different values are given for one coordinate here to represent the different boundaries for membrane/feed and membrane/permeate. To distinguish between these two boundaries, we name them $y = 1^+$ and $y = 1^-$ (the detailed description of such boundary condition can be found in Fluent user's guide 6.3.14.3.7 [24].). In our simulation, $y = 1^+$ corresponds to the membrane/feed interface and $y = 1^-$ corresponds to the membrane/permeate interface. Thus $T(x^*, 1^+)$ corresponds to $T_{f,m}(x)$, and $T(x^*, 1^-)$ corresponds to $T_{p,m}(x)$, as shown in Fig. 2.

The membrane interface of the permeate channel ($0 \leq x^* \leq \frac{l_{ch}}{h_{ch}}$, $y^* = 1^-$)

$$u^*(x^*, 1^-) = 0 \tag{36}$$

$$v^*(x^*, 1^-) = -\frac{J}{u_i \rho} \tag{37}$$

$$- k^* \frac{\partial T^*}{\partial y^*}(x^*, 1^-) = -\frac{h_{ch}(q_v^{''} + q_c^{''})}{k_i(T_{f,i} - T_{p,i})} \tag{38}$$

As discussed above, $y = 1^+$ corresponds to the membrane/feed interface and $y = 1^-$ corresponds to the membrane/permeate interface here. Thus $T(x^*, 1^-)$ corresponds to $T_{p,m}(x)$ as shown in Fig. 2.

The wall ($0 \leq x^* \leq \frac{l_{ch}}{h_{ch}}$, $y^* = 0$ and $0 \leq x^* \leq \frac{l_{ch}}{h_{ch}}$, $y^* = 2$)

$$u^* = 0 \tag{39}$$

$$v^* = 0 \tag{40}$$

$$- k^* \frac{\partial T^*}{\partial y^*} = 0 \tag{41}$$

$$D^* \frac{\partial w^*}{\partial y^*} = 0 \tag{42}$$

5. Special considerations for high temperature DCMD

5.1. System pressurization

To keep the feed and distillate from boiling if the temperature raised above the boiling point (such as ~102 °C for 3.5% concentration seawater at atmospheric pressure), the fluid is pressurized. This is included in the model but also has implications on the membrane structure and consequent effects on the transport through it, which are addressed in Section 5.2.

The dimensionless pressure, p^*, is nondimensionlized with respect to the saturation vapor pressure of the feed inlet, defined here as:

$$p^* = \frac{P}{p_{sat}} \tag{43}$$

$p^* = 2$ is the default setting.

An essential requirement for the membrane used in MD is that it must sustain the liquid/gas interface and prevent liquid from penetrating into the membrane pores. The "Liquid Entry Pressure" (LEP) is the maximal pressure difference across the pore liquid/gas interface that a membrane can sustain without allowing liquid penetration into the pore, and can be calculated using Young-Laplace eq. [2]:

$$LEP = \Delta P_{\text{inter}} = \frac{-2 B \gamma_L \cos \theta}{r_{\text{max}}} \tag{44}$$

where ΔP_{inter} is the pressure difference across the liquid/gas interface that, B: pore geometric coefficient (= 1 for cylindrical pores, assumed here), γ_L: the liquid surface tension, θ: the contact angle, and r_{max} is the maximal radius of the pore.

It is thus the pressure difference across the liquid/gas interface that affects the wetting, rather than the applied absolute pressure, so raising the absolute pressure of the streams at the membrane surface does not promote wetting as long as the LEP pressure difference is not exceeded, i.e., as long as the feed and the permeate streams are pressurized to the same extent, or even kept at a pressure difference below LEP, no wetting is expected to take.

To elaborate further, it is noteworthy here that the pressure difference across the membrane, and the liquid penetration into a pore and diffusion through it are also affected by the presence of air in the streams and pores. Our simulation model includes the presence of air in the membrane pores ((Eq. (11)) (primarily to include its effect on the distillate flux), and we assume that the total pressures of gas inside the pore is in equilibrium with the feed and permeate streams pressure. This is a widely used and justified assumption in modeling of DCMD [2], and the total pressure within the membrane equals to the pressure of the fluid, so if we pressurize the fluid to the same level on both sides, there is no LEP-affecting pressure difference across the membrane. Also, following Henry's ad Dalton's laws, the presence of air in the pores tends to lower the pressure difference across the gas/liquid interface, hence reducing the tendency for membrane wetting as also found both experimentally and theoretically by [25,26].

To determine the membrane interfacial pressure differences in the range of temperatures of our study and keeping in mind that the feed and permeate streams are in counterflow and in practice also use energy efficient heat recovery, the temperature differences between the feed and permeate streams are kept at about 10–15 °C, to maximize energy efficiency. The maximal vapor saturation pressure change with temperature, at 180 °C, is about 21 kPa/°C, so the maximal vapor pressure difference $\Delta P_{\text{interface}}$ under such practical counterflow conditions is about 315 kPa.

Using Eq. (11), we calculated the LEP for the membrane used in the simulation, which has a pore diameter of 0.27 μm, contact angle of 160 degrees (the ability to fabricate such superhydrophobic PTFE films having contact angles of 150–165 degrees was demonstrated [E.g. (27)], γ_L = 0.0474 N/m (extrapolated from data from [28]), and B = 1 (cylindrical pores), and found that LEP = 660 kPa. This is significantly higher than the above-determined maximal vapor pressure difference for typical operating conditions at the temperatures considered in this study, and supports the process feasibility.

Ultimately, these calculations serve well as feasibility evidence and guidelines for high temperature MD processes analyzed in the paper, but the real LEP behavior of MD membranes at given temperature levels and differences, and the effects of air on it, must be determined and verified experimentally under plant operating conditions.

5.2. Selection of membrane

As explained in Section 2.2 and quantified by Eqs. (2) and (4), the conductive fraction of the heat transfer across the membrane reduces the membrane energy efficiency and vapor mass flux. We consequently define the membrane thermal efficiency (η) as the ratio between the latent heat flux across the membrane due to solvent vaporization and the total heat flux across the membrane [11]:

$$\eta = \frac{J\Delta H_{fg}}{J\Delta H_{fg} + \frac{k_{me}}{\delta}(T_{f,m} - T_{p,m})} \tag{45}$$

It is noteworthy that the ideal value of η is equal to 1, i.e. when the entire heat flux is for the vapor transport through the membrane with none bypassed by conduction. Since this study focuses on investigating the potential for MD operation at temperatures higher than the currently used low ones, the first consideration for membrane material selection is the ability of these materials to operate well and robustly at the desired higher temperatures, but the above-described effect of membrane materials conductivity on membrane energy efficiency must be considered too. This is demonstrated well by the example that porous ceramic membranes, which have excellent tolerance to high temperature operation and have been studied and used, have thermal conductivities that are significantly higher than those of the polymers used in MD. The thermal conductivities of typically used polymers (polyvinylidene fluoride (PVDF), polytetrafluoroethylene (PTFE) and polypropylene (PP)) are in the range of around 0.1–0.5 W/(m·K) [2,6,27,28]. The ceramic membranes were generally fabricated from porous Alumina, Zirconia and Titania [31]. Alumina has a thermal conductivity around 30 W/(m·K). Zirconia has a thermal conductivity around 2 W/(m·K). Titania has a thermal conductivity around 10 W/(m·K). The ceramic membranes are made hydrophobic by surface-coating with hydrophobic material, such as PTFE.

Since high temperature DCMD will use membranes made of materials that may have thermal conductivities different than those commonly used in the current low temperature applications, it is now examined how this affects the system performance. Eq. (45) shows how the membrane material thermal conductivity influences the membrane thermal efficiency (η) of DCMD. Eqs. (2) to (11) and (45) show that the membrane thermal efficiency is a function of membrane properties r, ε, δ, χ, and k_s, and the temperature at the 2 liquid/membrane interfaces ($T_{f,m}$, $T_{p,m}$). We investigate here the influences of the membrane material thermal conductivity (k_s), membrane porosity (ε) and membrane feed side temperature ($T_{f,m}$) on the membrane thermal efficiency (η). The other parameters are kept constant at the values within the range of typical membranes used in MD [29], shown in Table 2 as a reference case to illustrate the influence of membrane thermal conductivity on membrane thermal efficiency.

Figs. 3 to 5 show the calculation results. It was found that for given $T_{f,m}$, η decreases significantly as k_s is increased since the conduction heat loss increases with k_s. According to Eqs. (2), (4), (8) to (11), given constant $T_{f,m}$ and other parameters in Table 2, $q_v^{"}$ does not change but $q_c^{"}$ changes linearly with k_s. For example for $\varepsilon = 0.5$, Eq. (45) shows

Table 2
Parameters for investigation of η.

δ (μm)	d_p (μm)	ε	χ	$T_{p, m}$ (K)
200	0.3	0.8	1.8	298.15
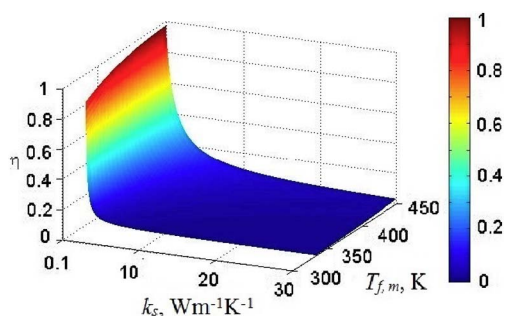
Fig. 3. The influence of k_s and $T_{f,m}$ on η, with $\varepsilon = 0.5$.
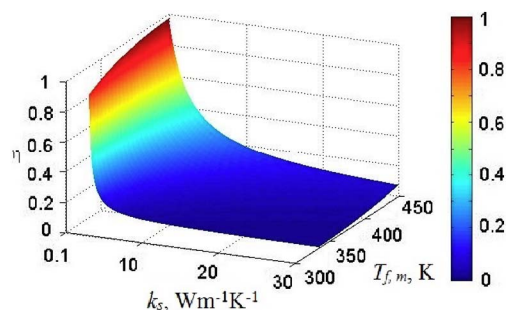
Fig. 4. The influence of k_s and $T_{f,m}$ on η, with $\varepsilon = 0.7$.
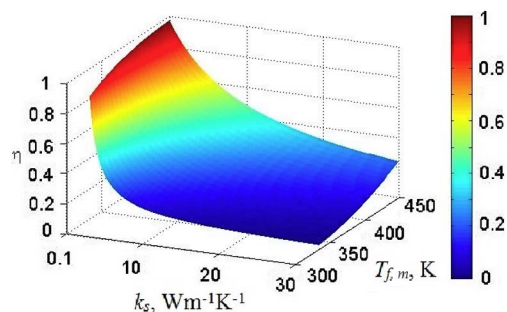

Fig. 5. The influence of k_s and $T_{f,m}$ on η, with $\varepsilon = 0.9$.

that increasing k_s from 0.1 to 10, causes $q_c^{"}$ to increases 50-fold and η to decrease 11-fold (from about 80% to 7.5%). For the same k_s, η increases with $T_{f,m}$, since the $q_v^{"}$ increases more rapidly compared with $q_c^{"}$ according to Eqs. (4), (8) to (11) and Ref. [30]. This is because the vapor pressure difference that is the driving force for J and $q_v^{"}$ increases more rapidly at higher temperature according to Eqs. (4), (8) to (11). Also, η decreases more significantly with the increase of the k_s for smaller values of ε, since for smaller ε, the k_s accounts for more of the effective membrane thermal conductivity (k_{me}), as Eq. (4) indicates.

To examine the performance of ceramic membranes for high temperature DCMD, the same simulation procedure to simulate the flat sheet DCMD module using the PTFE membrane is used except that $k_s = 2.0$ W/(m·K) which is the thermal conductivity of Zirconia and is the ceramic material with the smallest thermal conductivity among those discussed above. The other parameters are same for the flat sheet DCMD module using PTFE membrane and are listed in Tables 3 to 5. The results include $\eta = 17\%$ and $J = 0.009$ kg/(m²·s) since the temperature difference across the membrane is small due to high

Table 3
Membrane properties [9].

δ (μm)	d_p (μm)	ε	χ	k_s (W/(m·K))
205	0.27	0.47	2	0.15

Table 4
Module geometries.

l_{ch} (m)	h_{ch} (m)
0.1	0.001

Table 5
The base-case operating conditions.

$T_{f,i}$ (K)	w_i (%)	$u_{f,i}$ (m/s)	$T_{p,i}$ (K)	$u_{p,i}$ (m/s)
433.15	3.5	0.2	298.15	0.2

conductivity of the membrane material and the average temperature difference across membrane ($T_{f,m} - T_{p,m}$) is only 21.5 K. Relative to the results using a PTFE membrane under same conditions (shown in further below Section 8.1), use of the ceramic membrane yields a 3-fold lower J and 5-fold lower η indicating that the performance of DCMD using ceramic membranes is relatively rather poor.

While polymeric membranes have low material thermal conductivities, the ones typically used for MD (e.g., PVDF, PP, PTFE) may suffer unacceptable degradation or decomposition at high temperatures. PVDF and PP have melting temperatures around 160 °C [32], so they are unsuitable for the high temperature operation of up to 180 °C that is considered in this study. PTFE, however, has a long term service temperature around 260 °C [32], and are thus considered to be possibly suitable for high temperature MD, and therefore used in this study.

In addition to operating at the elevated temperatures considered in this study, the membranes must operate at the elevated pressures needed for avoiding boiling. It is important, therefore, to make sure that the membrane transport properties allow effective long-term operation under these conditions.

For example, compressive stresses may change the membrane porosity and tortuosity. In this study the required fluid pressure was between 200 kPa and 1960 kPa. Under the same compressive stress, the strain of PTFE increases with the increase of the temperature. The strain-stress curve in Ref. [33], shows that at 200 °C, PTFE can sustain a pressure of 2 MPa with a corresponding strain of 5.0%.and at 150 °C the strain corresponding to 2 MPa is only 2.5%, both very small that should not have a significant effect of on the membrane performance. We thus assumed that its geometric properties (ε, δ, χ, d_p) remain constant. The surface energy of solid materials also depends on the strength of the intermolecular bonds and the pressure, which, at least in the range relevant to this study, has little effect on their molecular structure. Furthermore, as the pressure is increased from atmospheric (100 kPa) to 1960 kPa, the surface tension of the water decreases by only 2% [34]. All this indicates that sufficient hydrophobicity can be maintained for the pressurized system.

A correlation from [35] is used to calculate the thermal conductivity within the temperature range investigate in this work by

$$k_s(T) = k_s(298K) \frac{1.0221 T_r^{0.1917} - 0.1959 T_r}{1.0221 T_{r1}^{0.1917} - 0.1959 T_{r1}} \tag{46}$$

where

$$T_r = \frac{T}{T_g} \tag{47}$$

$$T_{r1} = \frac{298}{T_g} \tag{48}$$

T_g for PTFE is 399.15 K, thus k_s changes only by 2% between 373.15 K to 453.15 K. Additionally, Eq. (4) shows that k_s accounts for only $(1 - \varepsilon)$ of the total k_{me}, so the change in k_s will results in only a 1% change of the k_{me} for a membrane with $\varepsilon = 0.5$, which is the membrane studied in this work, so k_s is considered to be constant in this work. Consequently, all the membrane properties are assumed to be constant in this work.

6. Modeling procedure

6.1. Default base-case parameter setting

The material properties of the flat membrane in this study, summarized in Table 3, were assumed to be the same as those of the tubular PTFE membrane used in [9]. Though the geometry of the membrane is different, they are in the range of commonly used flat sheet PTFE membranes [11].

A flat sheet DCMD module is simulated in this work. Fig. 1 shows the schematic of the DCMD module. The dimensions are given in
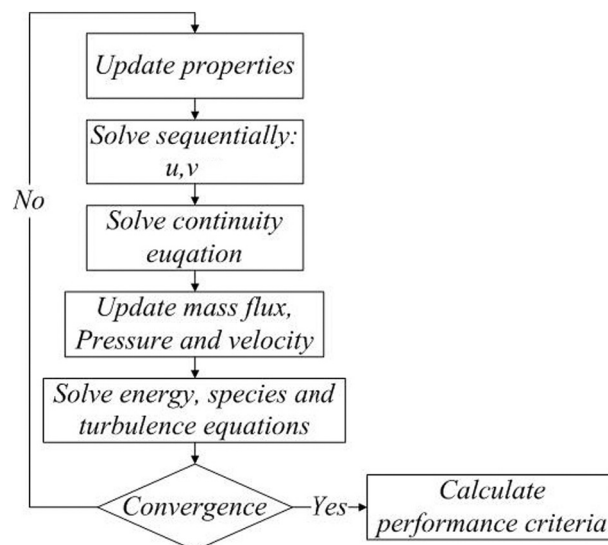
Fig. 6. Logic flow of the solution in Fluent.

Table 4.The geometry of this module is on the scale of the modules studied in [36–39].

The base-case operating conditions are given in Table 5. $T_{f,i}$ is chosen to be 433.15 K (160 °C), which is much higher than the feed temperature of conventional MD (that is about 353 K (80 °C)) and lies in the temperature range of our study. The $T_{p,i}$ is chosen to be 298.15 K, which is the ambient temperature, and w_i is chosen to be 3.5% typical to seawater. $u_{f,i}$ and $u_{p,i}$ are chosen to be 0.2 m/s which is comparable with the velocities used in [39–41]. The Re is about 2000 and a laminar flow model is used to simulate the process except in cases in which a turbulent model is specifically mentioned.

6.2. Method of solution, grid independence and validation

The simulation is carried out using the software Fluent 16.1 [24]. The pressure-based solver with SIMPLE scheme is chosen where the equations are solved in the procedure shown in Fig. 6. The second order upwind scheme is chosen to discretize the momentum, species and energy equations. High temperature results in large heat flux across the membrane and more drastic changes as a function of the feed temperature. This requires a computation mesh fine enough to capture such steep temperature changes and resolve them. The computational domain is divided into 50,000 cells, with 50 nodes used in the y direction and 1000 nodes in the x direction. The cells have an area of $4 \times 10^{-9} \text{ m}^2$. Increase of the number of cells from 50,000 to 200,000 resulted in only a 0.094% difference in the average total heat flux and 0.13% in the average mass flux, thus indicating that the grid was fine enough for this study.

The model (described in Section 2) validation for the DCMD operating below 100 °C is done first. The computed mass flux was compared with experimental results from Phattaranawik et al. [42] and Martinez et al. [43] at the same conditions they used, and was found to be in good agreement, within 9%, as Figs. 7 and 8 indicate. This comparison validates the correctness of the model used to describe the membrane, and the accuracy of the calculations for similar flow conditions.

The model is also approximately compared with the experimental results of Ref. [9]. Since we cannot model the complex module design and flow conditions in their work, their results are compared with our simulation using ideal conditions of no transport resistance of the flow ($\Omega = 0$). As shown in Table 1, their results show that when the feed temperature is raised from 108 to 118 °C, J increases from 68 to 115 kg/(m²·h) and the mass flux increase per degree temperature rise, ($\Delta J/\Delta T_{f,i}$), is 4.7 kg/(m²·h·°C). Our model has shown that raising the feed temperature from 108 to 118 °C resulted in an increase of J from
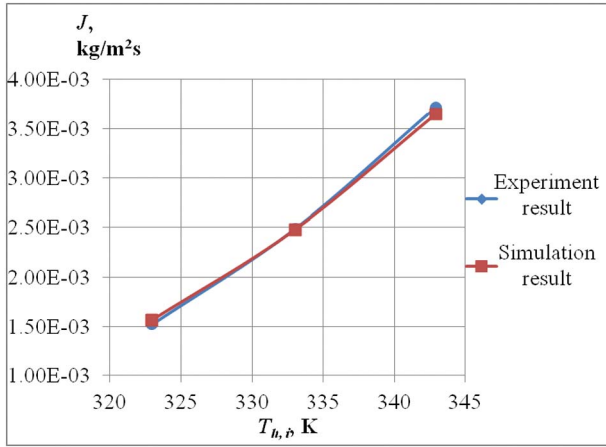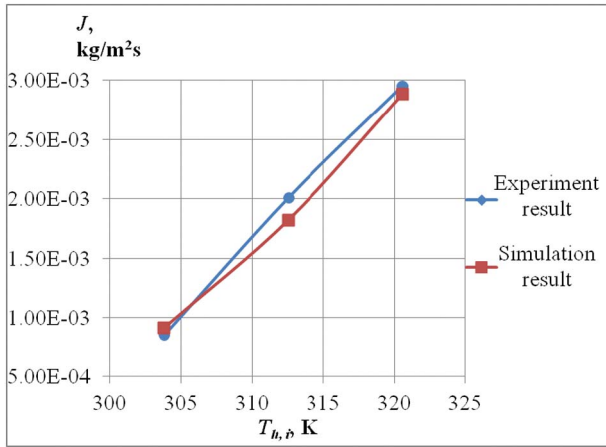
Fig. 7. The computed mass flux for different feed inlet temperature in this study, compared with experimental results from [42]. ($T_{p,i}$ = 20 °C, $u_{f,i}$ = 0.0632 m/s, $u_{p,i}$ = 0.0632 m/s, l_{ch} = 0.1 m, h_{ch} = 0.004545 m, δ = 126 μm, d_p = 0.22 μm, ε = 0.62, χ = 2, k_s = 0.041 W/(m·K)).

Fig. 8. The computed mass flux for different feed inlet temperature in this study, compared with experimental results from [43]. ($T_{p,i}$ = 14 °C, $u_{f,i}$ = 0.0635 m/s, $u_{p,i}$ = 0.0635 m/s, l_{ch} = 0.055 m, h_{ch} = 0.002 m, δ = 125 μm, d_p = 0.32 μm, ε = 0.75, χ = 1.7, k_s = 0.22 W/(m·K)).

86.9 to 136.5 kg/(m²·h) and in a mass flux increase per degree temperature rise, ($\Delta J/\Delta T_{f,i}$), of 5.0 kg/(m²·h·°C), very close to their results. Furthermore, it is reasonable that the simulation would give somewhat higher results than [9] because it was done for ideal conditions in which J and $\Delta J/\Delta T_{f,i}$, would indeed be higher. Altogether, these are quite satisfactory validations, especially when considering possible differences between the conditions used in our simulation model and those of their experimental study.

7. The used performance criteria

The main objective of separation processes, like MD, is to manufacture a desired product at minimal cost to production-rate ratio. Since this study does not address economic aspects, the major performance criteria chosen are those that evaluate the process water production rate, energy consumption and efficiency, and heat and mass transfer process foundations, as defined below. Detailed description and discussion of MD performance criteria was given by the authors in [11].

7.1. Mass flux (J)

Mass flux, the flux of the distillate vapor across a membrane, is the mass flow rate of the distillate across the membrane per unit membrane area:

$$J = \frac{\dot{m}_d}{A} \tag{49}$$

7.2. Membrane thermal efficiency (η)

The membrane thermal efficiency is defined as the ratio between the heat flux due to distillate evaporation and the total heat flux across the membrane:

$$\eta = \frac{q_v''}{q_t''} \tag{50}$$

7.3. Total heat flux (q_t'')

The "total heat flux" across a membrane is described by Eqs. (1) to (6).

7.4. Relative heat transfer resistance (Ω)

Based on the heat transfer resistance analog discussed in Section 2.2, the relative heat transfer resistance, Ω, is defined as the ratio of the convective heat transfer resistance to the total heat transfer resistance of the module and is calculated by

$$\Omega = 1 - \frac{T_{f,m} - T_{p,m}}{T_{f,i} - T_{p,i}} \tag{51}$$

7.5. Exergy efficiency (ψ)

Consideration of exergy and of its efficient use is important in all energy related processes, especially when more than a single type of energy is involved, such as the use of heat and pumping work as is the case in MD. The overall exergy efficiency of the DCMD module, ψ, in which the overall exergy destruction rate is $\dot{E}_{des}$, is defined here as the ratio of the exergy output of all energy outfows, $\dot{E}_{output}$ to the exergy input of all energy inflows, $\dot{E}_{input}$:

$$\psi = \frac{\dot{E}_{output}}{\dot{E}_{input}} = 1 - \frac{\dot{E}_{des}}{\dot{E}_{input}} \tag{52}$$

Detailed description of methods used to calculate exergy are given in [44,45], and of exergy efficiency of DCMD in [11]. The dead state for the exergy calculations is chosen here as T_0 = 298.15 K, p_0 = 101.325 kPa, and seawater solutes mass fraction $w_{s,o}$ = 0.035 kg/kg. To simplify the analysis, the permeate side temperature T_p is assumed to be the dead state temperature T_0.

7.6. Specific exergy consumption (SXC)

It is defined as the amount of exergy supplied to produce a unit mass of the product.

$$SXC = \frac{\dot{E}_{input}}{\dot{m}_{pro}} \tag{53}$$

As discussed in Ref. [11], the temperature and pumping pressure contribution to exergy are both included.

7.7. Specific energy consumption (SEC)

It is defined as the amount of energy supplied to produce a unit mass of the product.

$$SEC = \frac{\dot{E}_{input}}{\dot{m}_{pro}} \tag{54}$$

The energy input (Eq. (55)) for the module studied in this study is the heat supplied to the feed solution (Eq. (56)), and the pump work for pressurizing (by Δp) and driving the liquids (Eq. (57)).

The energy input to the module studied in this work is the sum of the heat needed to raise the temperature of a unit mass of fluid from ambient to the process inlet value, and the pumping work needed for that fluid to be pressurized from ambient pressure to the process inlet required value (Δp):

$$\dot{E}_{input} = \dot{E}_{heat} + \dot{W}_{pump} \tag{55}$$

The heat input rate needed to heat a stream having volumetric flow rate $\dot{V}$ is;

$$\dot{E}_{heat} = \dot{V}\rho C_p (T_{f,i} - T_0) \tag{56}$$

For a pump of efficiency γ, the pump work needed to pressurized the fluid is calculated by

$$\dot{W}_{pump} = \dot{V}(P_{f,i} - P_0)/\gamma \tag{57}$$

It is noteworthy that while pumping work for stream pressurization for high temperature operation somewhat increases with the pressure, it is well established that typically the pump work required for DCMD is only a small fraction of the heat demand ($\sim 0.5\%$) and if ever warranted by economic considerations, very high pressure stream energy could be recovered by pressure work exchangers.

8. Results and discussions

8.1. Effect of the feed inlet temperature

As presented in the Introduction (Section 1), the mass flux and thermal efficiency of DCMD increase with the feed flow temperature, and we thus investigate the performance of DCMD with the feed inlet temperature up to 180 °C, well above the commonly used maximal temperature of about 80 °C. The effects of the feed inlet temperature on the DCMD performance criteria are computed in the simulation and shown below.

Figs. 9 to 15 show the relative heat transfer resistance (Ω), the mass flux (J), the membrane thermal efficiency (η), the total heat flux ($q_t^{\prime\prime}$), the specific energy consumption (SEC), the specific exergy consumption (SXC) and the exergy efficiency (ψ) with default parameters setting listed in Tables 3 to 5, except that $T_{f,i}$ is varied.

As $T_{f,i}$ is increased from 353.15 K to 453.15 K:

- Ω increases by 54%, since the temperature polarization is intensified at higher temperature as reported in [1].
- J, η and $q_t^{\prime\prime}$ increase, as expected: J 9.4-fold, η 2.1-fold and $q_t^{\prime\prime}$ 4.5-
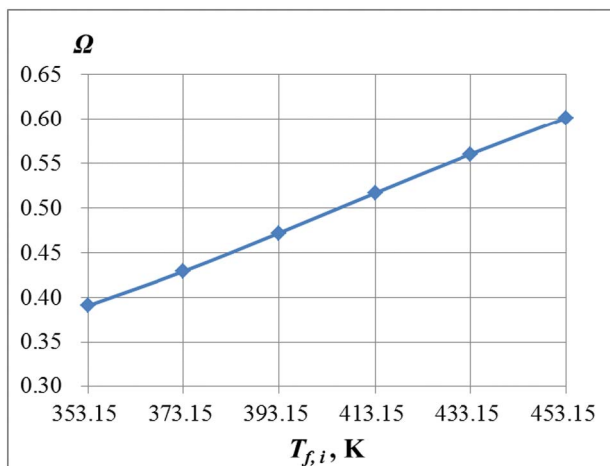
Fig. 9. The relative heat transfer resistance (Ω) as a function of $T_{f,i}$.
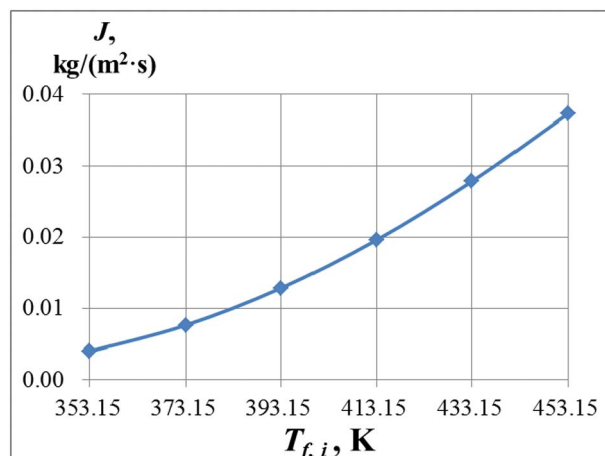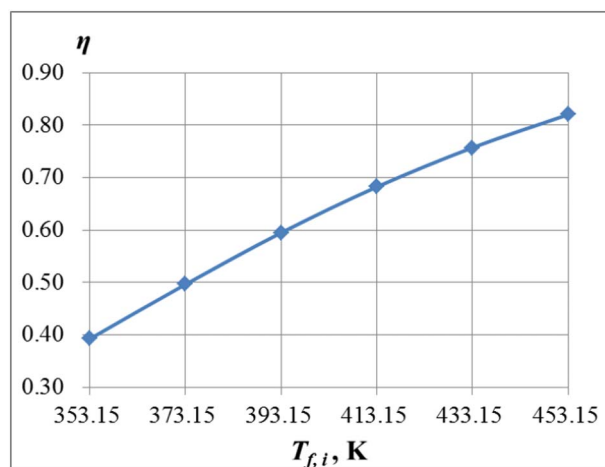
Fig. 10. The mass flux (J) as a function of $T_{f,i}$.

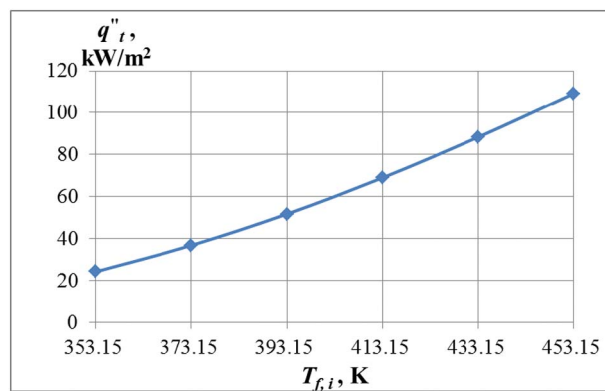Fig. 11. The membrane thermal efficiency (η) as a function of $T_{f,i}$.

Fig. 12. The total heat flux ($q_t^{\prime\prime}$) as a function of $T_{f,i}$.

fold, because increasing $T_{f,i}$ increases $T_{f,m}$ and thus the temperature difference ($T_{f,m} - T_{p,m}$) across the membrane and also the $q_t^{\prime\prime}$, J, and η according to Eqs. (2) to (11).

- SEC and SXC decrease by 2.9-fold and 1.4-fold, respectively, since J increases more significantly than the increase of exergy and energy inputs. As the $T_{f,i}$ is raised from 80 °C to 180 °C, J increases 9.4-fold, but the exergy input and energy input increase about 6.8-fold and 2.8-fold, respectively.
- Exergy is carried out by the feed stream since it has high temperature. As $q_t^{\prime\prime}$ increases, the drop of the outflow temperature of the feed
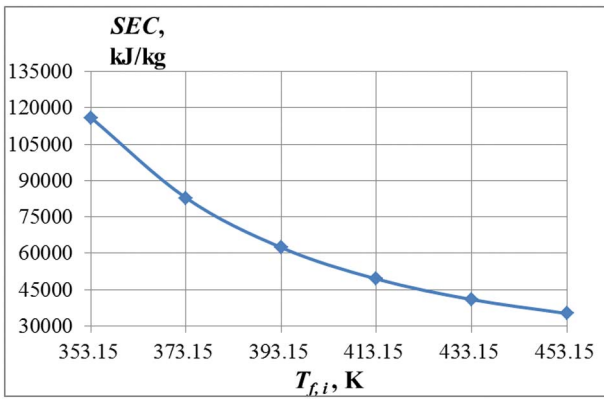
Fig. 13. The specific energy consumption (SEC) as a function of $T_{f,i}$.

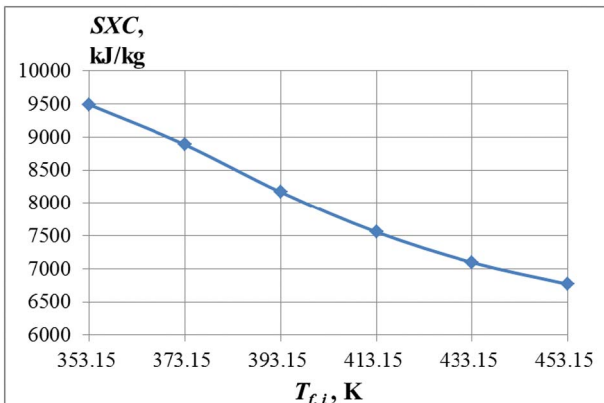Fig. 14. The specific exergy consumption (SXC) as a function of $T_{f,i}$.
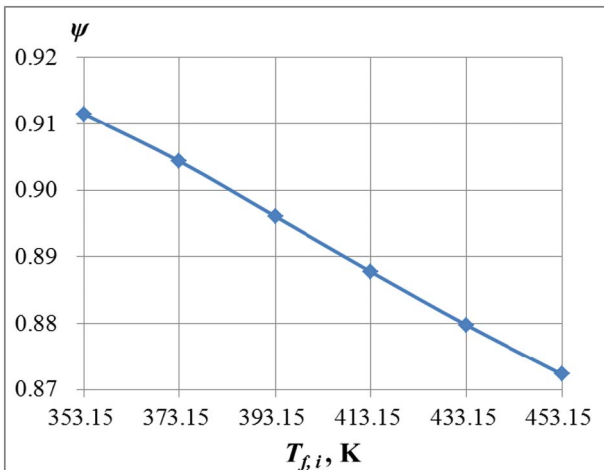

Fig. 15. The exergy efficiency (ψ) as a function of $T_{f,i}$.

Fig. 16. The temperature as a function of y^* at fixed $x^* = 50$ for $T_{f,i} = 353.15$ K.
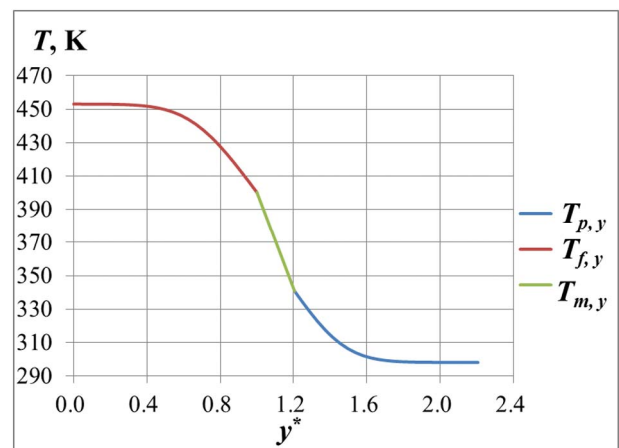
Fig. 17. The temperature as a function of y^* at fixed $x^* = 50$ for $T_{f,i} = 453.15$ K.

figures also show the fluid/membrane interface temperature and the temperature polarization there.

Figs. 18 and 19 show $T_{f,m}$ ($y^* = 1^+$) and $T_{p,m}$ ($y^* = 1^-$) along the membrane for $T_{f,i} = 353.15$ K and $T_{f,i} = 453.15$ K. Recalling that $y = 1^+$ corresponds to the membrane/feed interface and $y = 1^-$ corresponds to the membrane/permeate interface in the fluid computational domain. Thus $T(x^*,1^+)$ corresponds to $T_{f,m}(x)$, and $T(x^*,1^-)$ corresponds to $T_{p,m}(x)$ as shown in Fig. 2.

Fig. 18. The $T_{f,m}$ and along membrane/feed interface ($y^* = 1^+$) and $T_{p,m}$ along membrane/permeate interface ($y^* = 1^-$) for $T_{f,i} = 353.15$ K.

stream increases and the exergy of it decreases. As a result, ψ_R decreases by 4%.

• ψ_R decreases by only about 4% but the exergy input increases about 6.8-fold, thus the exergy output (exergy of the feed and permeate outflows) increases 6.5-fold and the exergy of the feed outflow accounts for 98% to 99% of the total exergy output (exergy of the feed and permeate outflows). This indicates that the feed outflow has more flow exergy for higher temperature DCMD and good opportunity for recovery of the exergy of the feed outflow.

• The temperature profile depicted qualitatively in Fig. 2, is computed as a function of y^* at the module mid-length (at $x^* = 50$) and shown in Figs. 16 and 17 for $T_{f,i} = 353.15$ K and $T_{f,i} = 453.15$ K. The
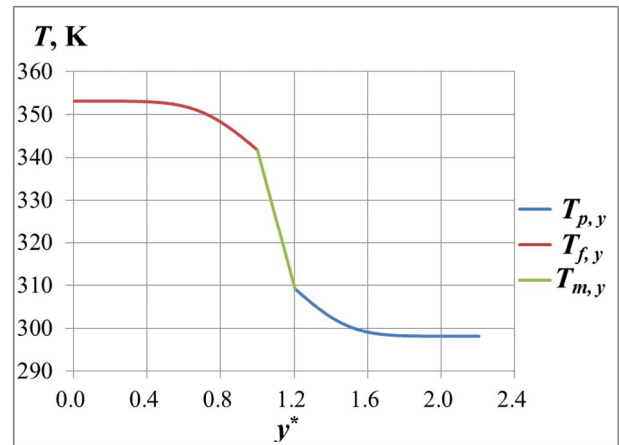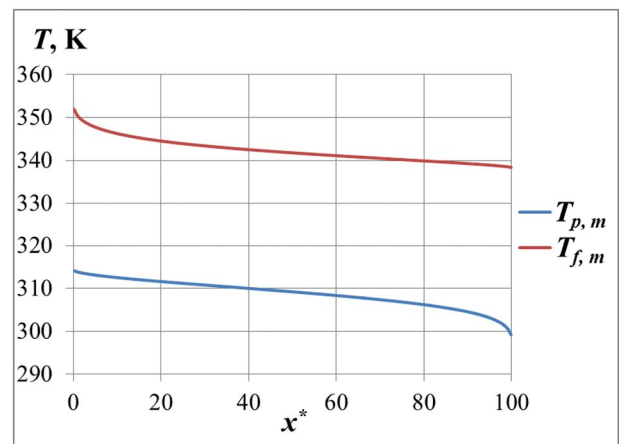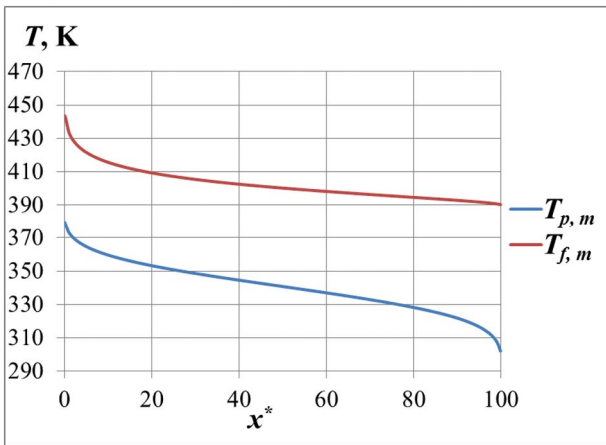
Fig. 19. The $T_{f,m}$ and along membrane/feed interface ($y* = 1^+$) and $T_{p,m}$ along membrane/permeate interface ($y* = 1^-$) for $T_{f,i} = 453.15$ K.

8.2. Effect of the Reynolds number (Re) of the feed and permeate streams.

It is known that transport with the fluid is improved by raising the *Re*, which influences the performance of MD by reducing the heat and mass transfer resistances and the polarization phenomena in the streams. The laminar flow model is used for *Re* ≤ 2000, and the turbulent for *Re* > 2000. The turbulent model is also intentionally extended to *Re* = 2000 to compare the results of laminar and turbulent flow models under the same condition. The effects of the *Re* are computed in the simulation and shown below.

Figs. 20 to 26 show the relative heat transfer resistance (Ω), the mass flux (*J*), the membrane thermal efficiency (η), the total heat flux (q_t''), the specific energy consumption (*SEC*), the specific exergy
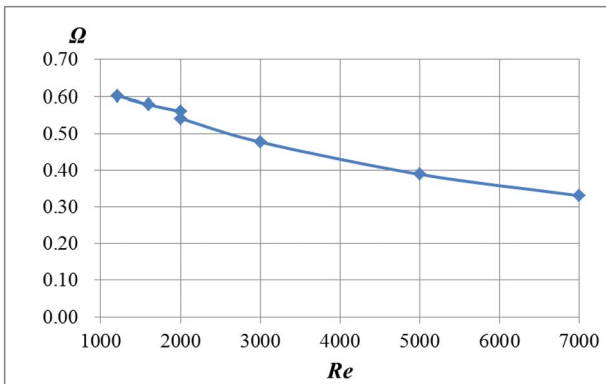

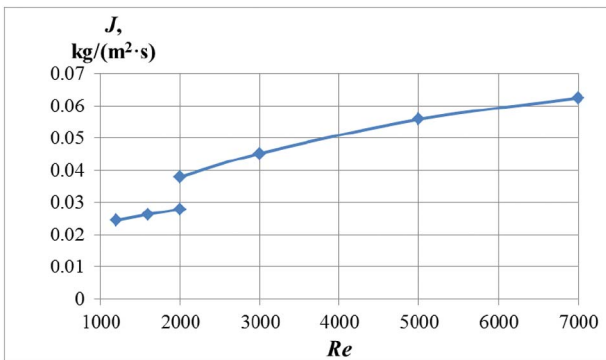Fig. 20. The relative heat transfer resistance (Ω) as a function of *Re* (laminar and turbulent).

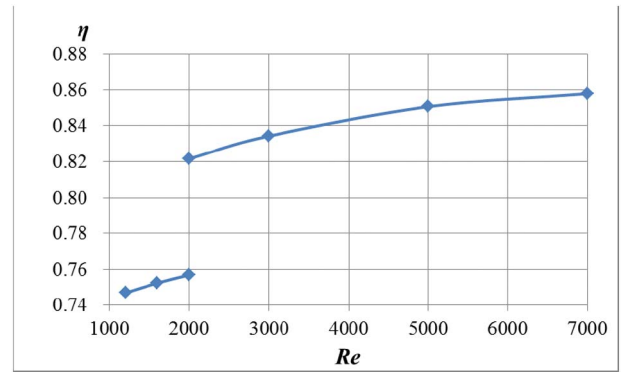Fig. 21. The mass flux (*J*) as a function of *Re* (laminar and turbulent).

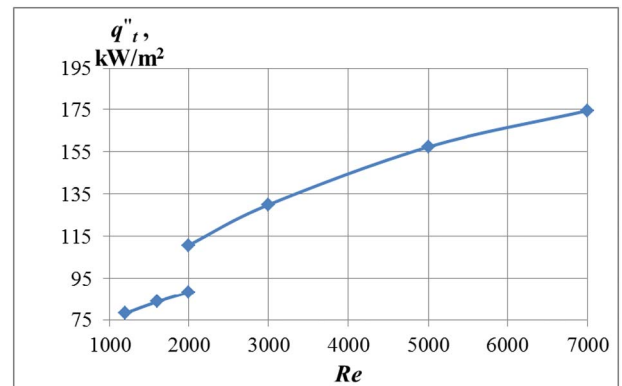Fig. 22. The membrane thermal efficiency (η) as a function of *Re* (laminar and turbulent).

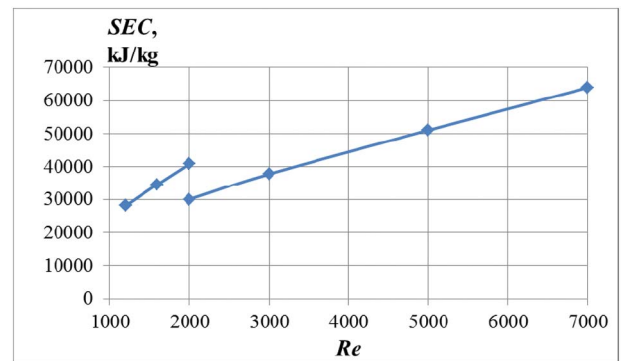Fig. 23. The total heat flux (q_t'') as a function of *Re* (laminar and turbulent).

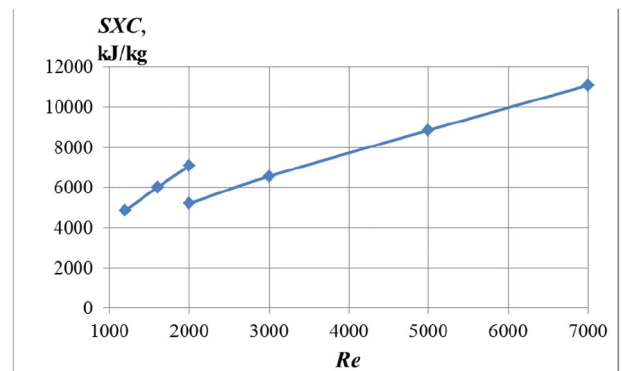Fig. 24. The specific energy consumption (*SEC*) as a function of *Re* (laminar and turbulent).

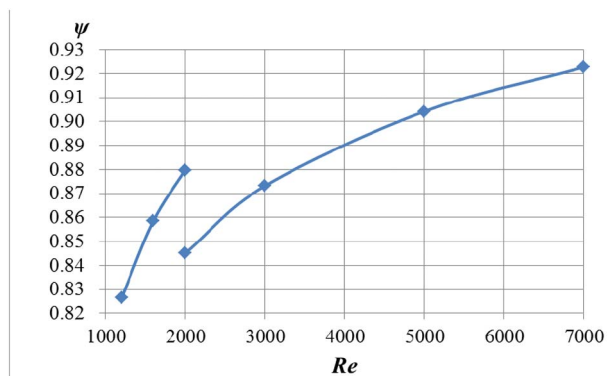Fig. 25. The specific exergy consumption (*SXC*) as a function of *Re* (laminar and turbulent).

Fig. 26. The exergy efficiency (ψ) as a function of Re (laminar and turbulent).

consumption (SXC) and the exergy efficiency (ψ) with default parameters setting listed in Tables 3 to 5, except that Re is varied in the laminar and the turbulent region.

As Re is increased 5.8-fold:

- Ω drops as expected, here by 55%, since increasing Re improves the transport with the fluid.
- J, η and $q_t^{"}$ increase, as expected. J increases 2.6-fold, η increases by 15% and $q_t^{"}$ increases 2.2-fold. This is because lower Ω means larger temperature difference ($T_{f,m} - T_{p,m}$) across the membrane and larger $q_t^{"}$, J, and η by Eqs. (2) to (11).
- SEC and SXC increase by 2.3-fold, since J increases less significantly than the increase of exergy and energy input. As the Re is raised from 1200 to 7000, J increases 2.6-fold, but the exergy input and energy input increase about 6.5-fold.
- ψ increases by 12%. Higher Re results in larger exergy input because of larger mass flow rate. The increases in exergy input exceeds the increases in exergy destruction because of better transport and larger $q_t^{"}$, thus ψ increases. As the Re is raised from 1200 to 7000, the exergy input increases 5.8-fold, and the exergy destruction increases about 2.6-fold.
- A step change drop is observed at $Re = 2000$ due to the transition of laminar to turbulent flow, where different models are used in each of these regimes. This step shows:
  ■ A drop in Ω by 3%, since turbulent flow improves the transport compare with laminar flow.
  ■ A rise in $q_t^{"}$, and J, η at the step change, as a result of lower Ω, J increases by 36%, η increases by 9% and $q_t^{"}$ increases by 25%.
  ■ A drop by 4% in ψ because of higher $q_t^{"}$.
  ■ A drop in SXC and SEC by 27%. The exergy and energy inputs are almost the same for the same Re, since the mass flow rate and the temperature of the fluid are the same. Thus they are inversely related to J, and J increases by 36%.
- As the Re is raised from 1200 to 7000, J increases 2.6-fold and η increases by 15%. To compare the effects of Re in conventional MD. We studied a case with $T_{f,i} = 353.15$ K which is a feed inlet temperature used in conventional MD with the other parameters kept at their default setting listed in Tables 3 to 5. When Re is raised from 1200 to 7000, the J of such a conventional process increases 1.8-fold and η increases by 8%. This enhancement is smaller than in higher temperature MD, confirming that significant performance improvement can be achieved by increasing Re in high temperature DCMD.
- It is noteworthy that as the Re is increased from 1200 to 7000, ψ increases by 12% and the exergy input increases 5.8-fold, thus the exergy output (exergy of the feed and permeate outflows) increases 6.5-fold and the exergy of the feed outflow accounts for 98% to 99% of the total exergy output (exergy of the feed and permeate outflows). This indicates that the feed outflow has more flow exergy for higher Re of higher temperature DCMD and good opportunity for

recovery of the exergy of the feed outflow.

8.3. Effects of pressure

As mentioned, higher operating temperature requires the raising of the pressure to prevent boiling, so the effects of the operating pressure are computed in the simulation and shown below.

Table 6 presents the relative heat transfer resistance (Ω), the mass flux (J), the membrane thermal efficiency (η), the total heat flux ($q_t^{"}$), the specific energy consumption (SEC), the specific exergy consumption (SXC) and the exergy efficiency (ψ) with default parameters setting listed in Tables 3 to 5, except that $p*$ is varied. It can be seen that Ω, J and ψ do not change, $q_t^{"}$ and η decrease within 2%, SEC and SXC increase within 2%. This indicates that the pressure levels needed for the DCMD operation between 0.91 MPa to 1.5 MPa, do not affect the process performance significantly.

9. Conclusions

The effects of raising the saline water feed inlet temperature up to 180 °C, well-above the commonly used MD temperatures, on the performance of DCMD flat sheet modules were investigated by comprehensive computational simulation.

- Significant performance improvements can be achieved by high temperature MD: when $T_{f,i}$ is raised from 80 °C to 180 °C, J increases 9.4-fold, η increases 2.1-fold, $q_t^{"}$ increases 4.5-fold, SEC decrease by 2.9-fold, and SXC decrease 1.4-fold, although Ω increases by 54%, and ψ decreases by 4%.
- Some performance improvements can be achieved by increasing the Re of high temperature DCMD. For $T_{f,i} = 433.15$ K, as the Re is raised from 1200 to 7000, Ω drops by 55%, J increases 2.6-fold, η increases by 15%, $q_t^{"}$ increases 2.2-fold, and ψ increases by 12%, but SEC and SXC increase 2.3-fold. For $T_{f,i} = 353.15$ K, when Re is raised from 1200 to 7000, J increases 1.8-fold and η increases by 8%, but SEC increases by 3.2-fold. This indicates that raising Re gives higher enhancement in high temperature DCMD than in conventional lower temperature DCMD.
- The system pressurization needed for high temperature DCMD operation at $T_{f,i} = 433.15$ K in the investigated range of parameters is 0.91 MPa to 1.5 MPa, and it was found that it should not affect the process performance significantly; When the $p*$ is increased from 1.5-fold to 2.5-fold, Ω, J and ψ do not change, $q_t^{"}$ and η decrease within 2%, and SEC and SXC increase within 2%.
- To prevent membrane "wetting", the pressurization of the feed and permeate streams must be equal, or at least no more different from each other than the LEP. Ultimately, the calculations serve well as feasibility evidence and guidelines for high temperature MD processes analyzed in the paper, but the real LEP behavior of MD membranes at given temperature levels and differences, and the effects of air on it, must be determined and verified experimentally under plant operating conditions.
- Exergy analysis is performed for high temperature DCMD. When $T_{f,i}$

Table 6
Summary of the DCMD performance as a function of $p*$.

$p*$	Ω	J, kg/(m²·s)	η	$q_t^{"}$, kW/m²	SEC, kJ/kg	SXC, kJ/kg	ψ
1.50	0.56	0.028	0.76	88.81	40,395.41	7018.93	0.88
1.75	0.56	0.028	0.76	88.53	40,669.43	7062.79	0.88
2.00	0.56	0.028	0.76	88.33	40,879.96	7095.57	0.88
2.25	0.56	0.028	0.76	88.17	41,051.42	7121.55	0.88
2.50	0.56	0.028	0.75	88.05	41,192.30	7142.19	0.88

is increased from 80 °C to 180 °C, the exergy output (exergy of the feed and permeate outflows) increases 6.5-fold and the exergy of the feed outflow accounts for 98% to 99% of the total exergy output. When *Re* is increased from 1200 to 7000, the exergy output increases 6.5-fold and the exergy of the feed outflow accounts for 98% to 99% of the total exergy output. High temperature DCMD thus offers good opportunity for energy and exergy recovery from the hot concentrated feed outflow stream, and such designs should be developed.

- While typically available ceramic membranes for MD have good tolerance to high temperature operation, they also have high material thermal conductivities and thus have much poorer *J* and *η* than polymeric membranes.
- Appropriate system design and material selection is essential for the high temperature DCMD system to work under high pressure and temperature. The specific membrane fabrication for high temperature DCMD is of interest for better performance.
- Recognizing that high temperature MD is more vulnerable to precipitation of salts such as calcium carbonate, magnesium hydroxide, and calcium phosphate, if they are present in the feed water, which may cause excessive fouling of the membranes, we note that it can be used if the feed water does not originally contain such species, or by pretreating the feed water if it does.
- This study doesn't address economics, but it is noteworthy that while high-temperature operation MD membranes are likely to be more expensive than the conventional ones at this time, price depends on the demand for such membranes, and membrane technology development is advancing rapidly. Consequently, there is no evidence that such membranes would be too expensive in the future, especially if the process is much more efficient as this study predicted.
- The higher operating temperatures provide more practical opportunities for heat recovery, which could significantly further raise overall system efficiency; suitable designs are thus needed to recover the high exergy and energy of the outflow in high temperature MD.

Acknowledgment

References

[1] M.S. El-Bourawi, Z. Ding, R. Ma, M. Khayet, A framework for better understanding membrane distillation separation process, J. Membr. Sci. 285 (2006) 4–29.
[2] K.W. Lawson, D.R. Lloyd, Membrane distillation, J. Membr. Sci. 124 (1997) 1–25.
[3] A.M. Alklaibi, N. Lior, Membrane-distillation desalination: status and potential, Desalination 171 (2005) 111–131.
[4] A.M. Alklaibi, N. Lior, Comparative study of direct-contact and air-gap membrane distillation processes, Ind. Eng. Chem. Res. 46 (2007) 584–590.
[5] L. Martinez, F.J. Florido-Diaz, Theoretical and experimental studies on desalination using membrane distillation, Desalination 139 (2001) 373.
[6] A. Alkhudhiri, N. Darwish, N. Hilal, Membrane distillation: A comprehensive review, Desalination 287 (2012) 2–18.
[7] E. Drioli, A. Ali, F. Macedonio, Membrane distillation: recent developments and perspectives, Desalination 356 (2015) 56–84.
[8] D. Singh, K.K. Sirkar, Desalination of brine and produced water by direct contact membrane distillation at high temperatures and pressures, J. Membr. Sci. 389 (2012) 380–388.
[9] D. Singh, K.K. Sirkar, High temperature direct contact membrane distillation based desalination using PTFE hollow fibers, Chem. Eng. Sci. 116 (2014) 824–833.
[10] J. Lu, Y. Yu, J. Zhou, L. Song, X. Hu, A. Larbot, FAS grafted superhydrophobic ceramic membrane, Appl. Surf. Sci. 255 (2009) 9092–9099.
[11] A. Luo, N. Lior, Critical review of membrane distillation performance criteria, Desalin. Water Treat. (2016) 1–48.
[12] R.G. Munro, Evaluated material properties for a sintered a-alumina, J. Am. Ceram. Soc. 80 (1997) 1919–1928.
[13] L. Gazagnes, S. Cerneaux, M. Persin, E. Prouzet, A. Larbot, Desalination of sodium chloride solutions and seawater with hydrophobic ceramic membranes, Desalination 217 (2007) 260–266.
[14] Z.D. Hendren, J. Brant, M.R. Wiesner, Surface modification of nanostructured ceramic membranes for direct contact membrane distillation, J. Membr. Sci. 331 (2009) 1–10.
[15] S.R. Krajewski, W. Kujawski, M. Bukowska, C. Picard, A. Larbot, Application of fluoroalkylsilanes (FAS) grafted ceramic membranes in membrane distillation process of nacl solutions, J. Membr. Sci. 281 (2006) 253–259.
[16] A. Larbot, L. Gazagnes, S. Krajewski, M. Bukowska, K. Wojciech, Water desalination using ceramic membrane distillation, Desalination 168 (2004) 367–372.
[17] M.C. Duke, J. O'Brien-Abraham, N. Milne, B. Zhu, J.Y.S. Lin, J.C. Diniz da Costa, Seawater desalination performance of MFI type membranes made by secondary growth, Sep. Purif. Technol. 68 (2009) 343–350.
[18] K.J. Lu, J. Zuo, T.S. Chung, Tri-bore PVDF hollow fibers with a super-hydrophobic coating for membrane distillation, J. Membr. Sci. 514 (2016) 165–175.
[19] J. Zuo, S. Bonyadi, T.S. Chung, Exploring the potential of commercial polyethylene membranes for desalination by membrane distillation, J. Membr. S. 497 (2016) 239–247.
[20] D.M. Warsinger, J. Swaminathan, E. Guillen-Burrieza, H.A. Arafat, J.H. Lienhard, Scaling and fouling in membrane distillation for desalination applications: a review, Desalination 356 (2015) 294–313.
[21] L.D. Tijing, Y.C. Woo, J. Choi, S. Lee, S. Kim, H.K. Shon, Fouling and its control in membrane distillation—a review, J. Membr. Sci. 475 (2015) 215–244.
[22] S. Ebrahim, M. Abdel-Jawad, S. Bou-Hamad, M. Safar, Fifteen years of R & D program in seawater desalination at KISR part I. Pretreatment technologies for RO systems, Desalination 135 (2001) 141–153.
[23] M.H. Sharqawy, J.H. Lienhard, S.M. Zubair, Thermophysical Properties of Seawater: a Review of Existing Correlations and Data, 16 (2010), pp. 354–380.
[24] ANSYS, Inc., Fluent, (2016) (http://www.ansys.com/Products/Fluids/ANSYS-Fluent).
[25] R. Schofield, A. Fane, C. Fell, Gas and vapour transport through microporous membranes. II. Membrane distillation, J. Membr. Sci. 53 (1990) 173–185.
[26] R.W. Schofield, A.G. Fane, C.J.D. Fell, R. Macoun, Factors affecting flux in membrane distillation, Desalination 77 (1990) 279–294.
[27] Y. Zhang, Q. Ge, L. Yang, X. Shi, J. Li, D. Yang, E. Sacher, Durable super-hydrophobic PTFE films through the introduction of micro-and nanostructured pores, Appl. Surf. Sci. 339 (2015) 151–157.
[28] K.G. Nayar, M.H. Sharqawy, L.D. Banchik, Thermophysical properties of seawater: a review and new correlations that include pressure dependence, Desalination 390 (2016) 1–24.
[29] M. Khayet, Membranes and theoretical modeling of membrane distillation: a review, Adv. Colloid Interf. Sci. 164 (2011) 56–88.
[30] Y. Zhang, Y. Peng, S. Ji, Z. Li, P. Chen, Review of thermal efficiency and heat recycling in membrane distillation processes, Desalination 367 (2015) 223–239.
[31] L.M. Camacho, L. Dumée, J. Zhang, J. Li, M. Duke, J. Gomez, S. Gray, Advances in membrane distillation for water desalination and purification applications, 5 (2013), pp. 94–196.
[32] G. Wypych, Handbook of Polymers, ChemTec Publishing, 2012.
[33] P. Rae, D. Dattelbaum, The properties of poly (tetrafluoroethylene) (PTFE) in compression, Polymer 45 (2004) 7615–7625.
[34] R. Massoudi, A. King Jr., Effect of pressure on the surface tension of water. Adsorption of low molecular weight gases on water at 25. deg, J. Phys. Chem. 78 (1974) 2262–2266.
[35] J. Bicerano, Prediction of Polymer Properties, second ed., Marcel Dekker, New York, 1996.
[36] J. Phattaranawik, R. Jiraratananon, A.G. Fane, Heat transport and membrane distillation coefficients in direct contact membrane distillation, J. Membr. Sci. 212 (2003) 177–193.
[37] Y. Yun, R. Ma, W. Zhang, A.G. Fane, J. Li, Direct contact membrane distillation mechanism for high concentration NaCl solutions, Desalination 188 (2006) 251–262.
[38] S. Srisurichan, R. Jiraratananon, A.G. Fane, Mass transfer mechanisms and transport resistances in direct contact membrane distillation process, J. Membr. Sci. 277 (2006) 186–194.
[39] J. Phattaranawik, R. Jiraratananon, A.G. Fane, Heat transport and membrane distillation coefficients in direct contact membrane distillation, J. Membr. Sci. 212 (1–2) (2003) 177–193.
[40] Y. Yun, et al., Direct contact membrane distillation mechanism for high concentration NaCl solutions, Desalination 188 (1–3) (2006) 251–262.
[41] S. Srisurichan, R. Jiraratananon, A.G. Fane, Mass transfer mechanisms and transport resistances in direct contact membrane distillation process, J. Membr. Sci. 277 (1–2) (2006) 186–194.
[42] J. Phattaranawik, R. Jiraratananon, A.G. Fane, Effects of net-type spacers on heat and mass transfer in direct contact membrane distillation and comparison with ultrafiltration studies, J. Membr. Sci. 217 (2003) 193–206.
[43] L. Martinez, F.J. Florido-Diaz, Theoretical and experimental studies on desalination using membrane distillation, Desalination 139 (2001) 373.
[44] L. Fitzsimons, B. Corcoran, P. Young, G. Foley, Exergy analysis of water purification and desalination: a study of exergy model approaches, Desalination 359 (2015) 212–224.
[45] W.R. Dunbar, N. Lior, R.A. Gaggioli, Component Equations of Energy and Exergy, 114 (1992), pp. 75–83.